Ultrafast Polyene Dynamics in Solution: The Conformational Relaxation and Thermalization of Highly Excited *cis*-1,3,5-Hexatriene as a Function of Initial Conformation and Solvent

Neil A. Anderson, Stuart H. Pullen, Larry A. Walker, II, Joseph J. Shiang, and Roseanne J. Sension*

Department of Chemistry, University of Michigan, Ann Arbor, Michigan 48109-1055

Received: July 27, 1998; In Final Form: October 15, 1998

Femtosecond transient absorption spectroscopy has been used to investigate the ground and excited-state dynamics of *cis*-1,3,5-hexatriene (Z-HT) and 1,3-cyclohexadiene following excitation to the strongly allowed 1^1B state in cyclohexane and *n*-hexadecane solvents. The internal conversion from the excited state manifold to produce vibrationally excited ground electronic state Z-HT occurs with rates of ca. $2-4$ ps^{-1}. The relaxation of highly excited Z-HT is used to probe the solvent−solute interaction and the influence of solvent on the competition between thermalization and single-bond isomerization dynamics. The data are also used to compare and contrast the hexatriene relaxation as a function of solute initial conditions (cZc-HT vs tZt-HT). A formalism for transforming the observed spectral data into time-dependent photoproduct yields is developed. These data are then compared with time-dependent quantum yields obtained from a transition state, rate equation approach to modeling the anticipated population dynamics. The detailed analysis of the results presented here are compared with the analysis of Lochbrunner et al. [Lochbrunner, S.; Fuss, W.; Schmid, W. E.; Kompa, K.-L. *J. Phys. Chem. A* **1998**, *102*, 9334. In press.] for the conformational relaxation of highly excited Z-HT in ethanol. Although the conformational evolution observed in hexadecane and cyclohexane are similar, the decays of cZc-HT and cZt-HT appear to be substantially faster in ethanol. These results are discussed in the context of Kramers theory for condensed phase reaction dynamics.

I. Introduction

The detailed mechanism of chemical transformation in fluid environments remains among the most important current problems in chemistry. Extensive experimental and theoretical investigations have explored the influence of solvent−solute interactions on chemical reaction dynamics over a wide range of time scales. For reactions where the reactant, transition state and product are all nonpolar, the key solvent−solute interactions involve the influence of the solvent on energy redistribution and energy transport, as well as the frictional influence of solvent presence on bulk motion (i.e., change in shape) by a solute in the course of a chemical reaction.

The *trans* to *cis* isomerization reaction of electronically excited *trans*-stilbene has provided the paradigm for the investigation of solvent effects on reaction dynamics involving barrier crossing processes. The comprehensive investigation of this reaction has included a multitude of studies exploring the effects of temperature, viscosity, pressure and polarity on the reaction rate.[1] Most of these studies have explored and modeled the reaction dynamics in the context of Kramers theory for an activated reaction in the presence of a frictional force. All of the studies have assumed an electronically excited reactant molecule with vibrational, rotational, and translational degrees of freedom in thermal equilibrium with the surrounding solvent. Thus, the reaction rate constant is assumed to be time-independent, reflecting a thermally activated barrier crossing process. A similar thorough, although somewhat less extensive, investigation of the much faster *cis* to *trans* excited-state isomerization has also been carried out.[2,3]

The roles played by a solvent in both solvent-assisted intramolecular vibrational energy redistribution (IVR) and energy transfer to the surroundings (thermalization) have also been the subject of comprehensive investigations.[4−7] The interaction between a molecule and the surrounding solvent on a sub-picosecond and picosecond time scale plays a significant role in governing the internal energy redistribution and thermalization of excited product molecules. Polyatomic hydrocarbon molecules have been shown to undergo ultrafast (i.e., subpicosecond) energy randomization followed by a somewhat slower, 10−20 ps, approach to thermal equilibrium with the surroundings.[4−7] Although it is clear that most molecules undergo ultrafast solvent-assisted energy redistribution, several recent studies have shown that ultrafast energy randomization over *all* available degrees of freedom should not be assumed a priori.[8−11] Some vibrational modes, or sets of vibrational modes, may be isolated from the bath provided by the remaining internal degrees of freedom. The isolated modes will relax on a slower time scale, competitive with the overall thermalization process.

The efficacy of intra- and intermolecular energy flow ultimately controls many aspects of condensed phase chemical reactions. For ultrafast reactions, occurring on time scales of less than a few 10s of picoseconds, a separation of time scales for energy randomization, thermalization, and activated reaction will not be achieved. Modeling such reactions will require a thorough understanding of the rate and extent of solvent-assisted intramolecular vibrational energy redistribution in condensed phase polyatomic molecules, as well as an understanding of the conditions that validate or invalidate the assumption of ultrafast IVR. Of equal importance is the fact that the assumption of a

10.1021/jp983181o CCC: $15.00
Published on Web 12/05/1998

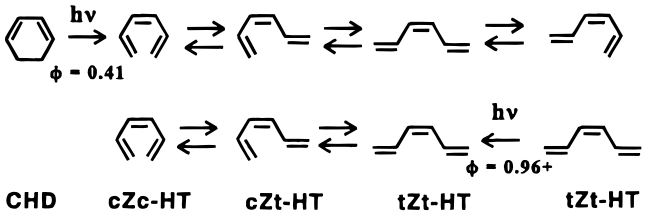

Figure 1. Diagram of CHD and the three rotamers of Z-HT.

time-independent rate constant for reaction will not be justified. The time-dependent internal energy content of the reactant molecule will result in time-dependent reaction rate constants. One of the key open questions in condensed phase chemical reaction dynamics involves the influence of time-variant non-equilibrium energy distributions on the observed reaction rates and product yields.

In the work reported here, the relaxation of highly excited *cis*-hexatriene (Z-HT) is used to probe the solvent−solute interaction and the influence of solvent on the competition between thermalization and single-bond isomerization dynamics. There is no evidence for a non-Boltzmann distribution of the available energy in Z-HT on time scales longer than a picosecond. Thus, these investigations are focused on the analysis of the observed conformational evolution under the assumption of ultrafast IVR.

II. Photochemistry of Cyclohexadiene and *cis*-1,3,5-Hexatriene

The development of versatile ultrafast lasers with wide wavelength tunability has provided a powerful tool for the investigation of chemical reaction dynamics in condensed phase systems. Recent work has explored the photochemistry and photophysics of the diene and triene chromophores that absorb strongly in the region around 260 nm. Experimental studies have examined the internal conversion and ground and excited-state dynamics of *cis*-1,3,5-hexatriene (Z-HT),[12−19] *trans*-1,3,5-hexatriene (E-HT),[12,14,18] 1,3-cyclohexadiene (CHD),[13,19−27] and 7-dehydrocholesterol.[28] The internal conversion process in these molecules is remarkably fast, necessitating reactive coordinates that require a minimum of nuclear motion, as well as powerful coupling mechanisms between the excited states. The potential energy surfaces responsible for internal conversion and excited state photochemistry have been investigated extensively on a theoretical basis by Robb and Olivucci and co-workers, using CASPT2 to search for pathways for nonradiative decay in the excited states of simple trienes and of cyclohexadiene.[29−36] These calculations have identified conical intersections that are easily accessible to the molecules in their excited states, facilitating extremely fast internal conversion.

Excitation of Z-HT or CHD in the allowed ultraviolet absorption band results in the production of vibrationally excited ground-state HT with a total excess vibrational energy of ca. 35000 cm^{-1}. The photoproduct in the ring-opening reaction of CHD is initially formed in a highly strained geometry, the di-s-*cis* conformer of hexatriene (cZc-HT), which will then undergo isomerization about the carbon−carbon single bonds as shown in Figure 1. Ab initio calculations predict that cZc-HT has a dihedral angle of ca. 40° about the central double bond, giving it a helical geometry, and significantly disrupting the π-conjugation in the molecule.[15] In contrast, hot HT produced following internal conversion of Z-HT will have an initial geometry similar to that of tZt-HT. Only a small amount of twisting around the single bonds is expected in the interval between excitation and internal conversion to the ground state potential energy surface via the conical intersections identified by Olivucci, Robb, and co-workers.

The ability to produce vibrationally hot HT with different initial energy distributions and different initial geometries provides an exceptional opportunity to explore the competition between conformational relaxation, intramolecular energy redistribution, and thermalization in condensed phases. The strong, structured UV absorption of Z-HT allows the use of ultrafast spectroscopic techniques to monitor the ensemble of photoexcited molecules along the approach to thermal equilibrium with the surroundings on the ground electronic state potential energy surface.

In previous papers we have used UV transient absorption spectroscopy to study the dynamics of Z-HT and CHD in cyclohexane solution both on the excited state and after ground state recovery.[15,24,27] Similar studies of Z-HT and CHD in ethanol solution have been presented by Lochbrunner et al.[19] In this paper we present complementary data for Z-HT and CHD in hexadecane solvent and compare and contrast the hexatriene relaxation as a function of solute initial conditions (cZc-HT vs tZt-HT) and as a function of solvent parameters. This paper also extends our previous analysis by presenting a formalism for transforming the observed spectral data into time-dependent photoproduct yields. These data are then compared with time-dependent quantum yields obtained from a transition state, rate equation approach to modeling the anticipated population dynamics.

III. Theoretical Background

In this section we develop the theory describing the time-dependent conformer populations. The most direct way to model the population dynamics in hot Z-HT is to make the assumption that the three conformational isomers represent distinct states where unimolecular rate constants may be defined for the transition from each conformer to the others. In this approximation, the relative populations of the conformational isomers (n_{cc}-(t), n_{ct}(t), and n_{tt}(t)) may be described by using coupled differential rate equations where the rate constants are a function of time due to the time-dependent energy content of the hot Z-HT molecule. The degeneracy of cZt-HT, resulting from the from the fact that either single bond can undergo isomerization, must also be accounted for in the calculation of the rate constants.

To model the time-dependent populations of the three conformers of Z-HT, it is necessary to derive an approximate expression describing the internal energy dependence of the rate constants for single-bond isomerization. For an isolated hot hexatriene molecule, assuming fast IVR, these rate constants may be expressed in terms of microcanonical transition state rate constants, $k(E)$, calculated, for example, by using Rice, Ramsperger, Kassel, Marcus (RRKM) theory, where the internal energy E is a slowly decaying function of time. For an isolated molecule in the absence of collisions, the only energy decay mechanism is radiative decay. In the high-pressure limit, where the collision frequency approaches infinity, the microcanonical rate constants may be used to calculate an average rate constant for a unimolecular reaction according to

$$\langle k \rangle = \int_0^\infty k(E)\, P(E)\, \mathrm{d}E / \int_0^\infty P(E)\, \mathrm{d}E \qquad (1)$$

where $P(E)$ is the distribution describing the fraction of molecules in the ensemble of reactant molecules having an energy E.

The proper description of $P(E)$ as a function of time following excitation is somewhat problematic. If there is no energy dissipation, the initial distribution is described by the equilibrium distribution of the reactant molecule prior to excitation translocated by the energy of the excitation photon:

$$P(E) = 0 \qquad E < h\nu_{\text{photon}} \tag{2}$$

$$P(E) = \rho(E - h\nu_{\text{photon}})\mathrm{e}^{-(E-h\nu_{\text{photon}})/k_{\text{B}}T_{\text{sample}}} \qquad E \geq h\nu_{\text{photon}}$$

where $\rho(E)$ is the molecular density of states at an energy E. As time proceeds, $P(E)$ will broaden and the peak will shift toward lower energies as interactions between the solvent and solute result in energy transfer and thermalization. Kaiser and co-workers have introduced the concept of internal temperature and have used this concept extensively to model vibrational cooling in polyatomic molecules.[5,6] For a molecule with harmonic vibrations, the maximum internal temperature T_{max} is the temperature which satisfies eq 3.

$$\bar{\nu}_{\text{photon}} + \langle E_{\text{init}} \rangle - \Delta H_{\text{rxn}} = \sum_{i=1}^{N_{\text{p}}} \frac{\bar{\nu}_i}{2} + \sum_{i=1}^{N_{\text{p}}} \bar{\nu}_i [\mathrm{e}^{\bar{\nu}_i/k_{\text{B}}T_{\text{max}}} - 1]^{-1} \tag{3}$$

In this equation, $\bar{\upsilon}_{\text{photon}}$ is the excess energy remaining in the molecule from the incident photon, ΔH_{rxn} is the enthalpy difference between the product and reactant molecules, the frequencies $\bar{\upsilon}_i$ are the N_{p} normal frequencies of the product molecule, and $\langle E_{\text{init}} \rangle$ is the average energy in a reactant molecule prior to excitation. The zero point energies are included explicitly in eq 3 to account for possible variations between reactant and product, particularly in the ring-opening reaction. The use of an internal temperature is a good approximation whenever $E_{\text{o}} \geq h\upsilon_i$ for all of the vibrational modes of the molecule.[5] This is clearly the case in the present set of experiments where $E_{\text{o}} \approx 37000\ \text{cm}^{-1}$ and $T_{\text{max}} \approx 2200$ K.[15,19,27]

Using the concept of internal temperature for hot Z-HT the unimolecular rate constant in eq 1 becomes the canonical transition state rate constant:

$$k_{\text{TST}}(T(t)) = \frac{k_{\text{B}}T(t)}{h} \frac{Q_{\text{TST}}(T(t))}{Q_{\text{r}}(T(t))} \mathrm{e}^{-E_{\text{a}}/k_{\text{B}}T(t)} \tag{4}$$

where Q_{TST} and Q_{r} are the vibration/rotation partition functions for the transition state and the reactant, respectively, and the temperature $T(t)$ is the time-dependent internal temperature of Z-HT. According to Kramers theory for unimolecular reactions in liquids,[37−39] transition state theory provides an upper limit for the rate constant with

$$k = k_{\text{TST}}\kappa_{\text{KR}} \tag{5}$$

where κ_{KR} is the Kramers transmission coefficient. The Kramer's coefficient may be approximated as[37−39]

$$\kappa_{\text{KR}} = \left[1 + \left(\frac{\beta}{2\omega_{\text{a}}}\right)^2\right]^{1/2} - \frac{\beta}{2\omega_{\text{a}}} \tag{6}$$

where ω_{a} is the (imaginary) frequency describing the curvature of the barrier between reactants and products and β describes the friction of the solvent on the reactive motion. In the high friction limit, eq 6 reduces to

$$\kappa_{\text{KR}} = \omega_{\text{a}}/\beta \tag{7}$$

To a first approximation, both ω_{a} and the friction coefficient β will be time independent. The friction coefficient will depend on the temperature of the surrounding solvent rather than the internal temperature of the solute. The temperature rise in the surrounding solvent will be relatively small and may be neglected. In the following analysis we will assume that $k_{\text{TST}}(T(t))$ depends on time through the time dependent internal temperature of the reactant molecule while the Kramers transmission coefficient is a time independent fitting parameter. Having made this assumption, it should be noted that Kramers theory itself will fail for reactions where the particle motion occurs on a time scale comparable to the solvent−solute force correlation time (typically ca. 0.1 ps).[39] An additional time dependence to the reaction rate constant may therefore arise from the failure of the Markovian, stochastic force approximation for highly excited Z-HT at early times.

The values of the time dependent rate constants calculated according to eq 4, and thus the time dependence of the cZc, cZt, and tZt populations, are very sensitive to the temperature dependence of the ratio of vibrational and rotational partition functions. The temperature dependent partition functions depend strongly on both the harmonic frequencies and the anharmonicities of the reactants (cZc, cZt, and tZt) and the two transition states. In the absence of high-quality potential surfaces we will make the common approximation that potentials are the same for the nonreactive coordinates for all three conformers and for the two transition states and use a harmonic potential for the reactive coordinate. The expression for the transition state rate constant then becomes:

$$k_{\text{TST}}(T) = \frac{k_{\text{B}}T}{h}[1 - \mathrm{e}^{-h\nu_{\text{a}}/k_{\text{B}}T}]\mathrm{e}^{-E_{\text{a}}/k_{\text{B}}T} \tag{8}$$

where υ_{a} is the frequency of the torsional mode in the reactant. A high-temperature approximation ($h\upsilon_{\text{a}} \ll k_{\text{B}}T$) is often made as a further simplification to eq 8:

$$k_{\text{TST}}(T) = \nu_{\text{a}}\mathrm{e}^{-E_{\text{a}}/k_{\text{B}}T} \tag{9}$$

The use of eq 9 removes all time and internal temperature dependence from the exponential prefactor. For the present analysis with $\bar{\upsilon}_{\text{a}} \approx 100-150\ \text{cm}^{-1}$, the exponential prefactor is expected to be temperature dependent. As approximated by eq 8, the exponential prefactor varies by 20−30% over the relevant temperature range from 300 to 2200 K. By using eq 8 rather than eq 9 to model the data, the frequency becomes a fitting parameter containing information about the ratio of the transition state and reactant partition functions, and compensating, at least partially, for the errors introduced by neglecting the total temperature-dependent partition functions in deriving eq 8 from eq 4.

The transient absorption measurements described in the next two sections and presented in our previous papers[15,24,27] will permit the extraction of time dependent quantum yields for cZc-HT, cZt-HT, and tZt-HT as described in section VI. These time-dependent quantum yields will be modeled by solving the coupled differential rate equations for the conformational populations with rate constants dependent on time through a time dependent internal temperature. The reactant frequencies and Kramers coefficients will be used as fitting parameters in the modeling.

IV. Experimental Section

The pump−probe transient absorption experiments reported here have been performed using an amplified, self-mode-locked

1 kHz Ti:sapphire laser. Both the laser system and the pump−probe experimental method have been described in detail previously.[15,40] Briefly, a Ti:sapphire oscillator is run at a fundamental wavelength in the 780−820 nm region, producing a pulse train of 20−30 fs pulses, at 100 MHz. A pulse picker is used to reduce the repetition rate to 1 kHz and the resulting pulse train is amplified using chirped pulse amplification in a Ti:Sapphire regenerative amplifier to pulse energies of ca. 400 μJ and pulse widths of 80 fs. In all of the pump−probe measurements reported here the pump frequency is the third harmonic of the femtosecond laser (ca. 0.5 μJ, 200 fs). The probe wavelength is generated by a variety of methods. For one-color experiments, the third harmonic was generated in both the pump and probe arms. The probe beam for two-color kinetics was generated by frequency doubling the visible output of an optical parametric amplifier (OPA) providing a ca. 200 fs, 0.2 μJ pulse in the 530−580 nm region. A pair of diodes were used to record absorption changes with narrow bandwidth probes.[15,40] Broadband spectra in the 265−300 nm region were also recorded with picosecond time resolution using a spectrometer and a UV sensitive CCD camera for detection.[15] The probe beam for these measurements was produced by focusing 1.5 μJ of the third harmonic into a 3 mm thick sapphire disk using a 25 mm focal length lens. Placing the sapphire at the focus generates a broadband ultraviolet continuum, stretching from 265 nm to beyond 300 nm.

Hexatriene was purchased as a mixture of *Z*- and *E*-isomers (Aldrich) and separation of the isomers was achieved using the method of Hwa et al.[41] Hexadecane, cyclohexane (both Aldrich, 99+% spectroscopic grade), and 1,3-cyclohexadiene (Aldrich) were used as purchased. The samples were prepared with an optical density of approximately 1.0 at 270 nm and kept in a temperature-controlled bath at 13.2 °C for the cyclohexane measurements, and 18 °C for hexadecane. The samples were circulated through a 1 mm path length flow cell (NSG) to refresh the volume between laser shots, and the sample reservoir was replaced periodically to avoid artifacts due to sample degradation.

V. Results

Time-Resolved Spectroscopy of 1,3,5-cis-Hexatriene. Kinetic data were obtained at seven probe wavelengths between 265 and 290 nm for *cis*-hexatriene in hexadecane solvent. Representative traces are presented in Supporting Information. Equivalent data for Z-HT in cyclohexane solvent has been presented previously.[15] All of the kinetics exhibit a spike at zero time delay corresponding to a solvent two-photon ionization. The intensity of the spike is linear with both pump and probe beam intensity, and it is only observed when the pulses are temporally overlapped. The spike is observed with no further dynamics in solvent-only scans, providing a cross-correlation of the pump and probe pulses.

Difference spectra at time delays of 5, 15, and 30 ps are shown in Figure 2. The 0−0 absorption of *cis*-hexatriene is bleached at all time delays, with significant absorption on the red edge. The absorption is broad enough to extend beyond our spectral window at early times. The bleach at 266−272 nm and the red-edge absorption both decay monotonically at most wavelengths over the time window presented. It is also notable that there is a distinct blue shift of the zero-crossing point at ∼270 nm as the time delay increases. This is evidence of the presence of a rotamer other than tZt-HT, as well as an indication of the strength of its absorption. For a vibrationally relaxed system with only cZt-HT and tZt-HT present, the zero-crossing point of the difference spectrum would correspond to the crossing point of the static absorption spectra of the two species. Vibrational cooling is not complete at 30 ps, but the blue shifting of the zero-crossing point with time indicates that the cZt-HT and tZt-HT spectra must cross at ∼270 nm. This suggests that the cZt-HT absorption has an intensity comparable to that of the tZt-HT 0−0 absorption band. The spectral data is qualitatively similar to that for *cis*-hexatriene in cyclohexane solvent (also shown in Figure 2).

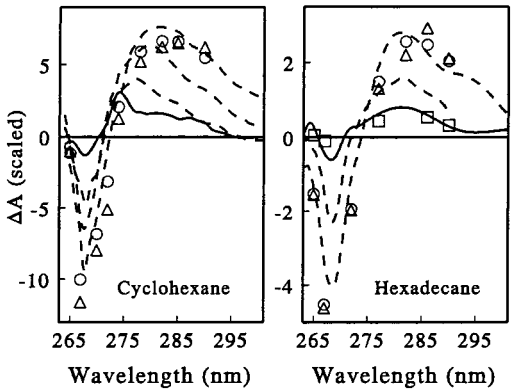

Figure 2. Difference spectra for cis-hexatriene in cyclohexane and hexadecane solvents. (a) Cyclohexane at 4, 10, 20, and 50 ps. The symbols represent data derived from the kinetic measurements at 0.5 (△) and 1.0 ps (○). (b) Hexadecane at 5, 15, and 30 ps. The symbols represent data derived from the kinetic measurements at 0.5 (△), 1.0 (○), and 50 ps (□).

The early evolution of the transient absorption spectrum may be extracted from the kinetic traces. To do this, the magic angle kinetic data are scaled so that the intensity at each kinetic wavelength matches the progression observed in the spectra for each of the time delays we have available. The two-photon ionization spike establishes zero time delay in the kinetic data. Thus, spectra can simply be obtained by compiling kinetic data at the time delay of interest. This method can be used to generate spectra for time delays as early as 500 fs. At earlier times the contribution from the ionization spike in the kinetics dominates. Spectra generated from the kinetic data in this manner for Z-HT in cyclohexane and hexadecane are shown as the symbols in Figure 2. The evolution from 0.5 to 4 ps is highlighted in Figure 3 for Z-HT in cyclohexane.

The data presented here are qualitatively similar to the data obtained by Lochbrunner et al. for tZt-HT dissolved in ethanol.[19] In particular, the same blue shift of the zero-crossing point as a function of time is observed around 270−275 nm. Quantitatively however, there are important differences. The data obtained in ethanol exhibit a faster decay of the bleaching around the 0−0 transition. The data reported in ref 19 indicate a decay of ca. 35% within 5 ps, while a decay of ca. 25% is observed in cyclohexane and hexadecane. A similar difference is observed for the decay of the transient absorption signal around 282 nm. In addition, the magnitude of the residual absorption attributed to cZt-HT at 40 and 80 ps is substantially smaller in ethanol than in cyclohexane or hexadecane.

Time-Resolved Spectroscopy of 1,3-Cyclohexadiene in Hexadecane. Kinetic data for CHD in hexadecane have also been obtained at seven probe wavelengths between 263 and 290 nm. The data are similar to that presented earlier for CHD in cyclohexane.[24,27] Representative data are provided in Supporting Information. In this case the formation of *cis*-hexatriene with a 40% quantum yield[42] results in a substantial increase in the absorbance of the sample in the region characteristic of the tZt-HT 0−0 absorption band, 265−273 nm. However, the kinetics

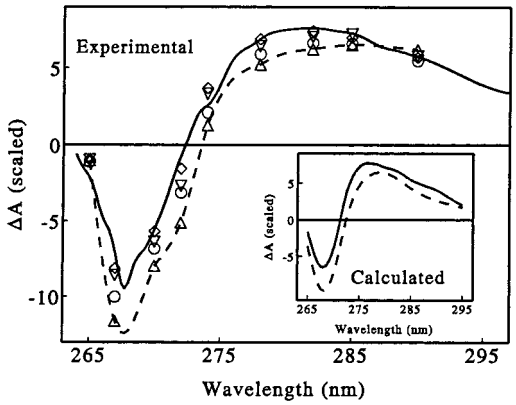

Figure 3. Evolution of the difference spectrum obtained following excitation of cis-hexatriene in cyclohexane from 0.5 to 4 ps. The symbols represent data derived from the kinetic measurements at 0.5 (△), 1.0 (○), 2.5 (▽), and 4 ps (◇). The dashed line is a cubic spline fit to the 0.5 ps data points. The solid line is the smoothed experimental difference spectrum measured 4 ps after excitation. The inset illustrates the expected evolution if 100% tZt-HT at 2000 K is converted to 70% tZt-HT at 1500 K and 30% cZt-HT. The calculation is performed as described in the text.

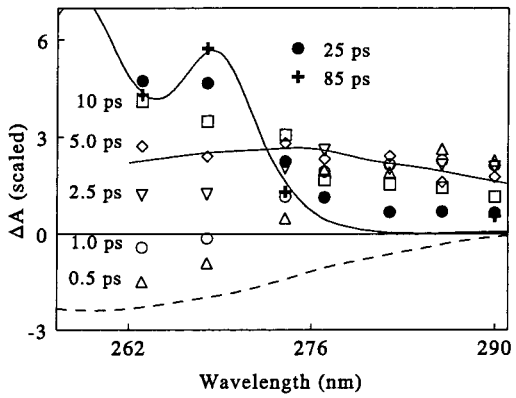

Figure 4. Difference spectra for cyclohexadiene in hexadecane derived from the kinetic measurements at 0.5 (△), 1.0 (○), 2.5 (▽), 5 ps (◇), 10 ps (□), 25 (●), and 85 (+) ps. The dashed line represents the bleach of CHD while the solid line represents the expected difference spectrum for the formation of Z-HT from CHD with a 40% yield. The flat solid line is the experimental difference spectrum observed at 5 ps.

at 263 and 268 nm exhibit a clear bleach in the first 1−2 ps, before developing a persistent absorption increase for longer time delays. The absorption grows to its maximum value at these wavelengths within 15−20 ps. As the probe wavelength increases, the contribution from the bleach of the CHD ground state decreases and the observed absorption reaches a maximum at earlier time delays. The initial absorption is then followed by some relaxation to a residual absorption, which is smaller in magnitude at the longer probe wavelengths.

The complementary spectral data, shown in Figure 4 clearly demonstrate the spectral evolution from a broad, structureless absorption to a spectrum very similar to tZt-hexatriene by 25 ps. The 0−0 band of the Z-HT absorption spectrum develops on a ca. 10 ps time scale. Data for CHD in cyclohexane was presented earlier,[27] and a slightly modified evolution is presented in Supporting Information. The spectrum of the initial photoproduct observed following excitation of CHD may be extracted from the data obtained 0.8 ps following excitation. This spectrum is shown in Figure 5 for excitation of CHD in cyclohexane[27] and hexadecane. There is no significant solvent dependence observed in the photoproduct absorption spectrum.

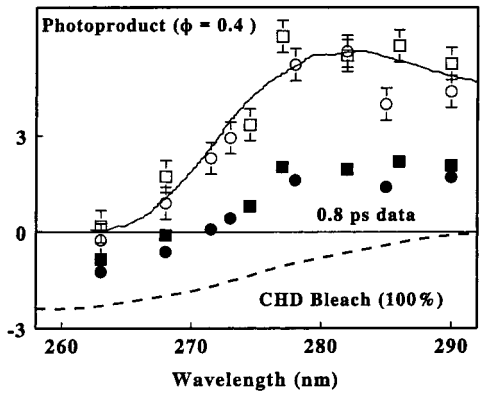

Figure 5. Comparison of the spectrum of the initial photoproduct observed in cyclohexane (circles) and hexadecane (squares). The filled symbols represent the raw data at 0.8 ps, while the open symbols represent the deduced photoproduct spectrum.

Again, the data presented here are qualitatively similar to the data obtained by Lochbrunner et al. for CHD dissolved in ethanol,[19] although important quantitative differences are apparent. The transient absorption data between 270 and 255 nm are uniformly positive by 0.9 ps following excitation for CHD dissolved in ethanol. In contrast, a clear bleach persists for 1−2 ps in cyclohexane and hexadecane. In addition, the magnitude of the red-edge absorption as a function of time relative to the intensity of the 0−0 transition at 80 ps is consistently smaller in ethanol than in cyclohexane or hexadecane.

VI. Discussion

Excited-State Dynamics. For Z-HT and CHD in both of the solvents studied, multiexponential modeling of the kinetic data requires a sub-picosecond time constant. These rates are not required to fit the data at all wavelengths, but are critical to a correct modeling of the data at several key wavelengths. Our data is best fit with rates of ca. 2 to 4 ps^{-1} for CHD and Z-HT. The assignment of the fast component observed following excitation of Z-HT to internal conversion from the 2 ^{1}A state to the ground electronic state is now well established.[12−19] The identification of the initial photoproduct following excitation of CHD is somewhat more ambiguous. The initial time-resolved resonance Raman studies of the CHD ring-opening reaction yielded a 6 ps time constant for the appearance of the ground state photoproduct, deduced primarily from the rise time of the strong 1625 cm^{-1} ethylenic stretching vibration.[20−23] A two-component analysis of the time-resolved resonance Raman data indicates the presence of a "dark" state having a lifetime of ca. 6 ps which decays to form the observed photoproduct. A three-component analysis of the data indicates the presence of a dark state which decays to form an observable photoproduct (υ = 1610 cm^{-1}) on a 5 ps time scale and which in turn decays to form a secondary photoproduct (υ = 1625 cm^{-1}) on a 7 ps time scale. Reid et al. assigned the dark state as the 2^{1}A excited electronic state implying a ca. 5 or 6 ps internal conversion to the ground electronic state.

Transient absorption studies in the UV spectral region in several different solvents demonstrate that the initial photoproduct formed following excitation of CHD has a broad red-shifted absorption spectrum appearing on a time scale of ca. 300 fs (See Figures 4 and 5). The appearance of the initial photoproduct is essentially identical in hexadecane (present work), cyclohexane,[27] and ethanol,[19] although the decay is somewhat faster in ethanol than in hexadecane or cyclohexane. The initial photoproduct observed in the transient absorption

measurements must correspond to the dark state in the resonance Raman experiment. The assignment of this state to cZc-HT or 2^1A_1 is not straightforward, however.

Recently, vapor phase REMPI and intense-field ionization experiments have suggested a sub 100 fs time constant for the decay of the excited electronic state and a ca. 200 fs time constant for the rise of signal attributed to the initial cZc-HT photoproduct in the vapor phase.[13,25−26] In the experiments of Fuss et al., the photoproduct state is observed to have a lifetime in excess of 700 ps.[25] This precludes assignment of this state to the 2^1A_1 state in the vapor phase. In accord with the ultrashort excited state lifetime inferred from the ionization measurements, the initial photoproduct observed in solution phase has also been assigned to cZc-HT.

As pointed out by Lochbrunner et al.,[19] it is possible to reconcile the apparent ultrafast appearance of cZc-HT absorption with the slow appearance of the ethylenic stretching vibration in the time-resolved resonance Raman measurements. The intrinsic resonance Raman cross section for cZc-HT should be substantially lower than that of tZt-HT as a consequence of the lower oscillator strength for the absorption band. The oscillator strength for the $1^1A \rightarrow 1^1B$ transition of cZc-HT is calculated to be approximately a factor of 2 less than the same transition in cZt-HT and a factor of 4 less than the transition in tZt-HT.[24] The time-resolved resonance Raman measurements may not detect the initial cZc-HT photoproduct due to a lower intrinsic cross section, compounded by the broader band profiles expected for the initial very hot molecule. In this case, the two photoproducts in the resonance Raman measurements would be assigned to cZt-HT and tZt-HT, formed from the dark cZc-HT state on a 5-6 ps time scale.

Excess Energy and Internal Temperature. Before proceeding further in the analysis and discussion of the experimental data, it is useful to step back and consider the excess energy distribution which may be expected following ultrafast internal conversion to the ground electronic state. After excitation of Z-HT, highly excited Z-HT is returned to the ground state with ca. 37100 ± 800 cm^{-1} of excess energy. The precise energy content depends on the specific excitation wavelength, which varied from 273 to 262 nm in these experiments, and on the amount of energy which is lost to the solvent surroundings during the excited state lifetime. The 0−0 transition to the 2^1A state of Z-HT is believed to lie 5275 cm^{-1} below the 0−0 transition to the strongly allowed 1^1B state in the vapor phase molecule.[43] For the present set of measurements the excitation wavelength falls within ±800 cm^{-1} of the solution phase 0−0 transition. Therefore, during propagation on the 2^1A excited state surface, the excited molecule has an initial excess energy of 4500 to 6000 cm^{-1}. Assuming a standard relaxation time constant (8−12 ps) for simple hydrocarbons in solution,[4−7] the electronically excited Z-HT molecule will lose only 150 ± 50 cm^{-1} of the available excess energy to the surrounding solvent prior to internal conversion to the ground state surface. Thus, most of the available excess energy remains in the molecule and is dissipated to the solvent from Z-HT in the ground electronic state.

The vibrationally excited Z-HT produced following excitation of CHD will possess somewhat less excess energy as a result of the difference in energy of the two isomers. CHD is approximately 5300 cm^{-1} more stable than Z-HT.[44] Thus, excitation of CHD between 262 and 273 nm will produce Z-HT with 31800 ± 800 cm^{-1} of excess energy within a few hundred femtoseconds.

TABLE 1: Potential Parameters for the Ground Electronic State of *cis*-1,3,5-Hexatriene

species	relative energy (cm^{-1})	isomerization	barrier height (cm^{-1})
tZt	0	tZt → cZt	1809
tZt/cZt TS	1809		
cZt	1088	cZt → tZt	721
		cZt → cZc	2282
cZt/cZc TS	3370		
cZc	2956	cZc → cZt	414

TABLE 2: Estimated Temperature for the Initial Z-HT Photoproducts

	CHD → product		tZt-HT → product	
photoproduct	$\langle E_{excess} \rangle$ (cm^{-1})	T_{max} (K)	$\langle E_{excess} \rangle$ (cm^{-1})	T_{max} (K)
cZc-HT	28400	1943	34000	2191
cZt-HT	30300	2029	35800	2271
tZt-HT	31400	2077	37000	2322

There are three spectroscopically distinct ground state rotamers of *cis*-1,3,5-hexatriene involving s-cis (or gauche) and s-trans conformations about the two carbon−carbon single bonds. To provide an estimate of the barrier for s-trans to s-cis isomerization in Z-HT, transition state calculations have been performed in Gaussian 94,[45] using restricted Hartree−Fock method with a 6-31G basis set. The results of these calculations were presented previously[15] and are summarized in Table 1. Our values for the properties of the rotamers are in good agreement with previous calculations on conjugated polyenes and are sufficient for a qualitative or semiquantitative description of the population dynamics.[46,47]

The Gaussian 94 calculations may also be used to describe the harmonic potential surface for vibrational motion in each of the three rotational conformations. The vibrational partition function for a harmonic oscillator may be used to describe, at least qualitatively, the energy distribution in a hot hexatriene molecule. The estimated maximum vibrational temperatures calculated for cZc-HT, cZt-HT and tZt-HT following excitation of CHD and tZt-HT by using eq 3 are tabulated in Table 2. In every case, the Z-HT is highly vibrationally excited with an initial vibrational temperature that is in excess of 1900 K.

In reality Z-HT is better described as an anharmonic oscillator than a harmonic oscillator. Most of the anharmonic couplings will be negative, resulting in an increase in the density of states as a function of energy. This increase in the density of states will have the result of lowering the effective temperature of the highly excited molecule below that expected based on the harmonic oscillator partition function. Therefore, the temperatures in Table 2 should be considered as upper limits only.

Experimental Time Dependence of the cZt-HT Population following tZt-HT Excitation. In both the ring-opening reaction of cyclohexadiene[24,27] and the relaxation dynamics of *cis*-hexatriene,[15] we have stressed that fitting the data to a sum of exponentials does not yield direct information about any single physical process other than return to the ground state. Instead, the data reveals a convolution of cooling and rotational isomerization processes.[15,24,27,48,49] Further, fitting the data to a model capable of describing the behavior of this system, incorporating the ultrafast excited state decay and the following single-bond isomerization dynamics, would require too many variables to yield a meaningful result.

A different approach must therefore be taken. The spectrum of cZt-HT can be extracted from the 50 ps difference spectrum for Z-HT in cyclohexane. This experimental spectrum was used as a standard because the thermalization of Z-HT is nearly

complete and no contribution from cZc-HT is expected. Equation 10 can be used to produce a trial spectrum of cZt-HT based on the 50 ps difference spectrum, by assuming a quantum yield of cZt-HT and a molecular temperature for tZt-HT.

$$A_{ct}(\lambda) = \frac{1}{\Phi_{ct}}[(1 - \Phi_{ct})\,(A_{tt}(\lambda, T) - A_{tt}\,(\lambda, 290\ \mathrm{K}) - \Delta A_{obs}(\lambda)] \quad (10)$$

where Φ_{ct} is the cZt-HT quantum yield at 50 ps, $A_{tt}(\lambda,T)$ is the molecular temperature-dependent absorption spectrum of tZt-HT, and ΔA_{obs} is the observed 50 ps difference spectrum. Varying the temperature at 50 ps, as well as the cZt-HT quantum yield at 50 ps allows a range of possible cZt spectra. For this analysis, we have investigated a simple exponential decay of the internal temperature (eq 11) as the cooling model:

$$T(t) = (T_{max} - T_{sample})e^{-t/\tau_{vib}} + T_{sample} \quad (11)$$

treating the cooling rate τ_{vib}^{-1} and cZt-HT quantum yield at 50 ps as the only parameters in the fitting. T_{sample} is the equilibrium temperature of the sample prior to excitation.

Generation of trial cZt-HT spectra using eq 10 produces some insight into the 50 ps quantum yield. The strength of the absorption in the 50 ps difference spectrum requires a major contribution from cZt-HT. Attributing this contribution to a quantum yield of <5% requires the absorption spectrum of the rotamer to be stronger than the absorption of the tZt-HT isomer, which is unreasonably strong for a nonplanar *cis*-rotamer.[24] This constraint allows these low quantum yields to be eliminated from further consideration.

The remaining potential cZt-HT spectra were then used to model the experimental data. Collection of time-resolved difference spectra at several time delays between 5 and 30 ps allowed the kinetic data to be placed on a common intensity scale. With eight kinetic probe wavelengths extending from 265 to 290 nm, a good estimate of the difference spectrum at any desired time delay is obtained by compiling the kinetic intensities at that delay. Spectra were generated in this manner for 13 time delays ranging from 5 to 30 ps.

Equation 12 was then used to generate a predicted difference spectrum at each time delay by calculating ΔA at each kinetic wavelength.

$$\Delta A(t,\lambda) = \Phi_{ct}(t)A_{ct}(\lambda) + (1 - \Phi_{ct})A_{tt}(\lambda,T(t)) - A_{tt}(\lambda,290\ \mathrm{K}) \quad (12)$$

$A_{ct}(\lambda)$ is simply the trial spectrum of cZt-HT generated from the 50 ps data. This analysis assumes a constant spectrum for cZt-HT regardless of vibrational excitation. This is a simplification, but the breadth and lack of major structure in the cZt-HT spectrum should render the differential temperature effects a minor correction to the increase in the red-edge absorption observed for vibrationally relaxed cZt-HT compared with tZt-HT. The tZt-HT spectrum as a function of temperature, $A_{tt}(\lambda,T(t))$, was calculated as described in our previous paper.[15]

In general, for molecules at the high initial temperatures expected following excitation of Z-HT or CHD, the possible contribution of intensity from the wing of higher energy electronic transitions should also be considered. For Z-HT the fully allowed transition from the ground state to the 1^1B state has maximum Molar extinction coefficient of 4.1×10^4 $M^{-1}cm^{-1}$ at 258 nm (38 800 cm^{-1}).[50] No other intense transition is observed in the solution phase spectrum (λ > 190 nm). The next absorption band with significant intensity in the gas phase spectrum falls at 155 nm with a maximum Molar extinction coefficient less than 0.3 times that of the strong UV transition.[51] Thus, contributions to the transient absorption between 250 and 300 nm from higher electronic states of Z-HT are expected to be insignificant.

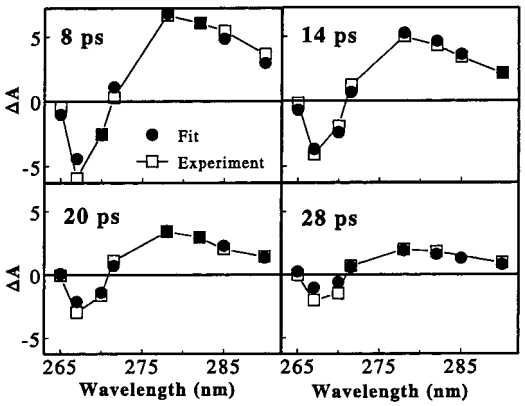

Figure 6. Comparison of the fitted (filled circles) and experimental (open squares) difference spectra in cyclohexane at four delay times for the best fit cooling rate and cZt-HT quantum yields as discussed in the text.

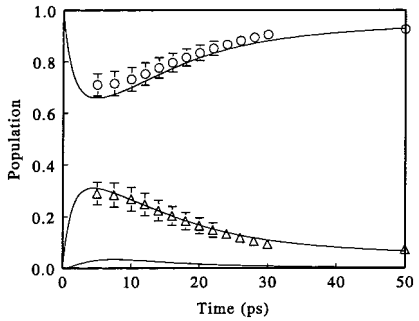

Figure 7. Quantum yields for cZt-HT (triangles) and tZt-HT (circles) in cyclohexane as a function of time after excitation of tZt-HT under the assumption that only these two species contribute to the observed difference spectra. The error bars represent the range of quantum yields determined for cooling time scales of 12 ± 3 ps and 50 ps cZt-HT yields of 7 ± 2%. The solid lines represent the populations calculated as a function of time for tZt-HT, cZt-HT, and cZc-HT according to the model discussed in the text.

The experimental difference spectra were fit by using eq 12 and allowing the cZt-HT quantum yield at each time delay Φ_{ct}-(t) to vary freely. The quality of spectral fits at the 13 different time delays was used to determine the combination of cooling rate and 50 ps cZt-HT quantum yield which produced the best overall fit to experiment. Cooling rates ranging from 4 to 20 ps were tested, yielding a best-fit cooling rate of 12 ± 3 ps. The 50 ps cZt-HT quantum yield is estimated to be 7 ± 2% for *cis*-hexatriene in cyclohexane. Comparisons of the fitted and experimental difference spectra are shown in Figure 6.

Figure 7 shows the estimated quantum yields as a function of time based on this analysis. The quantum yield for cZc-HT is about 30% at 5 ps, and falls steadily to 7% at 50 ps. In the case of Z-HT, the initial population of cZt-HT upon return to the ground state will be minimal, and the rise in the magnitude of the transient absorption signal in the first 5 ps results from energy randomization in the molecule and from the rapid buildup of the cZt-HT population. The possible presence of cZc-HT should also be noted. However, cZc-HT is highly energetically unfavorable, lying 1816 cm^{-1} higher than cZt-HT. If cZt-HT only builds up to around 30% of the total, then cZc-HT should only be a small fraction of that number and can effectively be ignored.

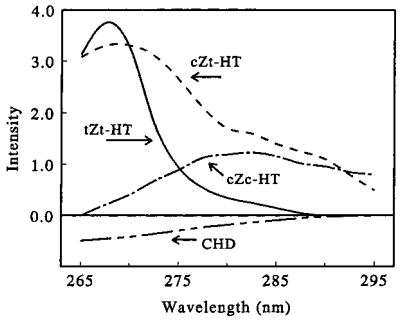

Figure 8. Spectra of the conformers of Z-HT deduced from the present set of experiments. These spectra are used to model the evolution following excitation of CHD. The contribution due to the bleach of CHD is also indicated.

Figure 3 illustrates a comparison of the observed transient difference spectra at 0.5 and 4 ps with difference spectra predicted according to the analysis described above. At 0.5 ps essentially all of the photoproduct is expected to be tZt-HT with an internal temperature of ca. 2000 K, while at 4 ps the photoproduct is expected to consist of ca. 70% tZt-HT at 1500 K and 30% cZt-HT. The overall cooling of the sample gives rise to the initial decrease in the bleaching signal around 268 nm, while the conversion of tZt-HT to cZt-HT gives rise to the increase in the red-edge absorption.

Rotamer Dynamics following CHD Excitation. The ring opening of CHD to form Z-HT with a 40% quantum yield was also investigated in both cyclohexane and hexadecane solvents. A quantitative analysis of the rotamer dynamics following CHD excitation is complex; however, qualitative population behavior can be extracted under the postulate of a three-state system:

$$\Delta A(t,\lambda) = \Phi_{cc}(t)A_{cc}(\lambda) + \Phi_{ct}(t)A_{ct}(\lambda) + \Phi_{tt}A_{tt}(\lambda) - A_{CHD}(\lambda) \quad (13)$$

where the total population of Z-HT, $\Phi_{cc}(t) + \Phi_{ct}(t) + \Phi_{tt}(t)$ at any time after internal conversion to the ground state is constant. CHD molecules that undergo reaction will likely return to the ground state in a cZc-HT configuration. Thus, the initial photoproduct spectrum following excitation of CHD provides an estimate of the cZc-HT spectrum as discussed previously.[27] The cZt-HT spectrum has been estimated from the transient difference spectrum obtained following excitation of tZt-HT as discussed above and in ref 15. The tZt-HT spectrum is obtained from the steady state UV−vis spectrum. These three spectra are shown in Figure 8, along with the contribution due to the bleaching of CHD.

Estimates of the time-dependent quantum yields for the three conformers may now be extracted from the data by fitting the experimental difference spectra (see Figure 4a) using eq 13. The results of such an analysis for the data obtained in cyclohexane solvent is shown in Figure 9. The large uncertainties indicated by the error bars result from the inherent uncertainties in the spectra of cZc-HT and cZt-HT and from neglecting of the effect of internal temperature on the spectra.

A few features of the population dynamics illustrated in Figure 9 should be noted. The slow decay of cZc-HT is necessitated by the slow rise of the difference spectrum in the region between 265 and 272 nm. The broad, flat transient difference spectra obtained 4 or 5 ps following excitation of CHD indicate that the population of the initial transient species is still dominant at this time delay. The decay of the cZc-HT population and the rise of the total cZt-HT + tZt-HT population occurs with a time-constant of 7.5 ± 2 ps. This is in good agreement with the 6 ± 1 ps time constant reported by Reid et al. for the appearance of the strong 1625 cm^{-1} ethylenic stretch in the time-resolved resonance Raman data according to a two component analysis.

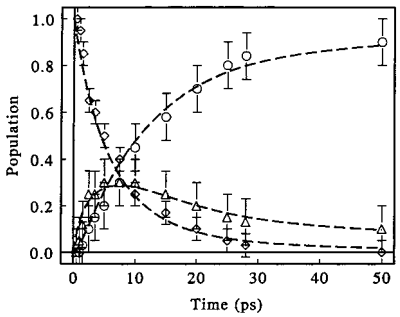

Figure 9. Quantum yields for cZc-HT (diamonds), cZt-HT (triangles) and tZt-HT (circles) in cyclohexane as a function of time after excitation of CHD under the assumption that dynamics are modeled as a three state system, neglecting the effect of temperature on the photoproduct spectra. The dashed lines represent the populations calculated as a function of time for tZt-HT, cZt-HT, and cZc-HT according to the model discussed in the text.

TABLE 3: Fitting Parameters for the Analysis of the Time-Dependent Conformer Populations in Cyclohexane

temperature decay	reactant coordinate	kramers coefficient
$T_{max} = 2000$ K	$\upsilon_{t\rightarrow c} = 90$ cm^{-1}	
		$\kappa_{tt-ct} = 0.2$
$\tau_{vib} = 12$ ps	$\upsilon_{ct\rightarrow tt} = 130$ cm^{-1}	
	$\upsilon_{cc\rightarrow ct} = 40$ cm^{-1}	$\kappa_{cc-ct} = 0.1$

Ground State Conformational Relaxation − Calculations. The observed conformational population dynamics may now be modeled by using the formalism described in section III above. The barriers and relative ground state conformational energies reported in Table 1 will be assumed to be accurate. As discussed previously, these quantities are in good agreement with experimental barriers, as well as barriers calculated using more sophisticated approaches.[15,52−54] Small changes in the parameters of the potential energy surface will result in small changes in the other fitting parameters, but they will not influence any of the qualitative conclusions.

The time-dependent population dynamics are modeled by numerical solution of the coupled differential rate equations using eqs 4 and 8, to calculate the rate constants as a function of the internal vibrational temperature. As above, an exponential decay of the internal temperature, which corresponds to an approximately exponential decay of the internal energy for a harmonic polyatomic molecule, will be assumed. The time constant for the temperature decay is 12 ps, as determined in the analysis of the time-dependent tZt-HT absorption. This temperature decay is consistent with the anti-Stokes time-resolved resonance Raman measurements of Reid et al. for Z-HT produced following excitation of CHD in cyclohexane.[22]

The lines in Figures 7 and 9 represent the population behavior predicted for the parameters listed in Table 3. The maximum transient quantum yield for cZt-HT following excitation of tZt-HT is strongly dependent upon the ratio of the vibrational partition functions for cZt and tZt-HT. The difference between the maximum quantum yield exhibited in Figure 7 and the maximum quantum yield calculated in our previous paper arises from the use in ref 15 of temperature-dependent vibrational partition functions and harmonic frequencies calculated in Gaussian 94. The high effective frequency for the cZt-HT → tZt-HT reaction coordinate reported in Table 3 is required by the relatively low peak yield observed in the data.

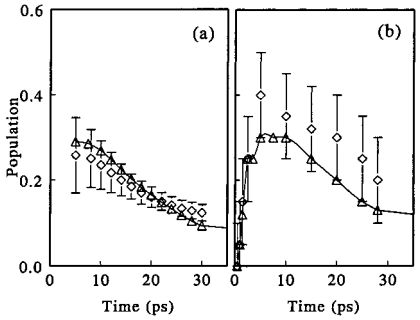

Figure 10. (a) Comparison of the estimated quantum yields for cZt-HT in cyclohexane (triangles) and hexadecane (diamonds with error bars) following excitation of Z-HT. (b) Comparison of the estimated quantum yields for cZt-HT in cyclohexane (triangles) and hexadecane (diamonds with error bars) following excitation of CHD.

The long decay of cZc-HT observed in the kinetic data following excitation of CHD and the slow rise observed in the time-resolved resonance Raman data of Reid et al.[20−23] necessitate the low Kramers coefficient for cZc-cZt isomerization and the low frequency of the reactant coordinate in cZc-HT. The cZc-HT population persists much longer than calculations would predict, based on the harmonic potential energy surface derived from the ab initio calculations. Given the uncertainties in the experimentally determined populations and the calculated energies, as well as the limitations of the model, the parameters in Table 3 should be considered only qualitatively accurate.

Solvent Dependence of the Isomer Population Dynamics. At this point it is interesting to look at the solvent dependence observed in the transient population data. The method of analysis developed above can be applied to investigate the effect of solvent viscosity on the cooling rate and population dynamics for the *cis*-hexatriene system. The Z-HT/hexadecane series of kinetics and spectra were scaled to be mutually consistent. The static absorption spectra of tZt in cyclohexane and hexadecane are virtually identical in our spectral window. It has therefore been assumed that the spectrum of cZt-HT calculated in cyclohexane can be used to closely approximate that in hexadecane. Use of the predetermined cZt-HT spectrum leaves the cooling rate as the only parameter in the analysis. A cooling rate of 12 ± 4 ps produces the best experimental fit for Z-HT in hexadecane. A comparison of the cZt-HT quantum yield as a function of time in the two solvents is shown in Figure 10. The population dynamics in both solvents appear to be nearly identical in their shape, with cZt-HT population peaking at about 5−8 ps and decaying steadily afterward. The two profiles are also quantitatively similar, although it appears possible that the population in hexadecane solution may peak slightly lower and the decay may be somewhat shallower than in cyclohexane.

The time-dependent populations for cZt-HT in hexadecane and cyclohexane following excitation of CHD are compared in Figure 10b. The data appear to support a larger transient yield for cZt-HT in hexadecane than cyclohexane. However, the difference falls within the error bars assigned in the analysis and may not be significant. The similarity in the behavior of Z-HT in cyclohexane and hexadecane following excitation of both CHD and Z-HT is highlighted by the 290 nm data. At this wavelength, there are no significant differences in the dynamics between the two solvents. Small differences are observed at other wavelengths.

The solvent trends observed in the time dependent cZt-HT populations extracted from the data are consistent with the expectations of Kramers theory, where the reaction rate constant will be inversely proportional to the friction on the reaction coordinate. In a hydrodynamic model, this friction will in turn be linearly proportional to the solvent viscosity. The observed data is clearly not consistent with a 3-fold reduction in κ_{KR} as estimated from the ratio of the macroscopic shear viscosity ($\eta_{chx} = 1.02$ cp (17 °C) vs $\eta_{hxd} = 3.34$ cp (20 °C)).[55] On the other hand, reduction of κ_{KR} for single-bond isomerization between cZt-HT and tZt-HT by ca. 25% from 0.2 to 0.15 may be supported by the data. The transient cZt-HT populations predicted for such variations in κ_{KR} are compared in Figure 11. A comparison of the transient population dynamics following excitation of CHD yields a similar conclusion for the solvent effect on the cZt-HT ⇄ tZt-HT isomerizations. A sublinear dependence of the solvent friction β on the shear viscosity η is not unexpected in the light of similar findings for stilbene isomerizations especially when disparate solvents are compared.[1−3]

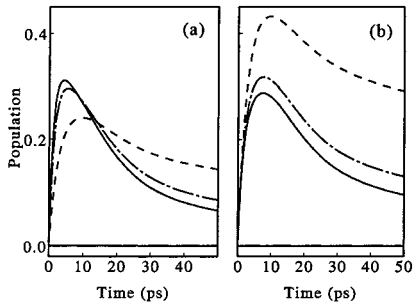

Figure 11. Dependence of the calculated transient population of cZt-HT following excitation of Z-HT (a) and CHD (b) on the value of κ_{KR} for the cZt-HT ⇄ tZt-HT isomerization coordinate. The values for κ_{KR} are dashed lines $\kappa_{KR} = 0.067$, dotted−dashed lines $\kappa_{KR} = 0.15$, and solid lines $\kappa_{KR} = 0.2$. The other parameters are as in Table 3.

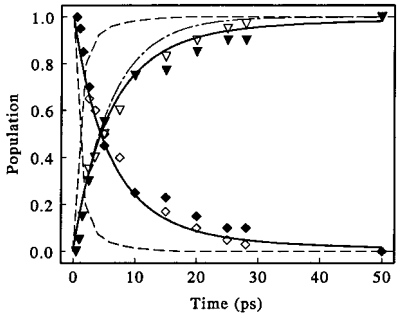

Figure 12. Comparison of the cZc-HT and (cZt-HT + tZt-HT) yields following excitation of CHD, as a function of solvent. The diamonds represent the relative population of cZc-HT in hexadecane (filled symbols) and cyclohexane (open symbols). The triangles represent the total population of cZt-HT and tZt-HT in hexadecane (filled symbols) and cyclohexane (open symbols). The solid lines represent the dynamics calculated by using the parameters in Table 3. The dot−dashed line represents a 6 ps appearance of Z-HT population as obtained from the time-resolved resonance Raman measurements of Reid et al.[22] The dashed lines represent the population dynamics deduced by Lochbrunner et al. in ethanol as reported in Figure 9 of ref 19.

Following excitation of CHD, analysis of the precise cZt-HT population as a function of time is hindered by the similarity in the cZt-HT and tZt-HT optical absorption spectra between 255 and 300 nm. It is, therefore, useful to compare data obtained in different solvents and by different techniques without attempting to separate the cZt-HT and tZt-HT populations. Figure 12 summarizes all of the available data for the decay of the cZc-HT population and the rise of the total cZt-HT + tZt-HT population following excitation of CHD in solution.

The data displayed in Figure 12 illustrate several important points: (1) A comparison of the decay of cZc-HT in cyclohexane and hexadecane may support a similar small (ca. 25%)

decrease in κ_{KR} for single-bond isomerization between cZc-HT and cZt-HT in hexadecane. A larger solvent induced decrease in the reaction rate is not supported by the data. (2) The rise of the total population of cZt-HT and tZt-HT in cyclohexane is entirely consistent with the time-resolved resonance Raman results of Mathies and co-workers if the dark state in the Raman experiment is assumed to be cZc-HT.[22] (3) Direct comparison of the 0.9 ps transient difference spectrum reported by Lochbrunner et al.[19] with the 1.0 ps spectra reported in Figure 6 indicates that the rate of decay of the cZc-HT conformer is much faster in ethanol than in cyclohexane or hexadecane. The magnitude of this difference is seen more clearly when the kinetic analysis used by Lochbrunner et al.[19] to predict the time-dependent population of cZc-HT in ethanol is compared with the population dynamics reported above (Figure 12).

A direct comparison of the value of $\kappa_{KR} = 0.25$ to 0.30 reported in ref 19 with values reported above is inappropriate due to the differences in the calculations. However, the population dynamics illustrated in Figure 9 of ref 19 may be reproduced reasonably well by using $\tau_{vib} = 7$ ps and $T_{max} = 2400$ K as assumed by Lochbrunner et al., the reaction coordinate frequencies listed in Table 3 and $\kappa_{KR} = 0.4$ for both reaction coordinates. This represents a ca. 4-fold rate enhancement for the cZc-HT → cZt-HT isomerization in ethanol as compared with cyclohexane or hexadecane. The solvent dependence of κ_{KR} clearly cannot be described by using a hydrodynamic model for the solvent friction as the viscosity of ethanol is somewhat larger than the viscosity of cyclohexane. A sample temperature is not reported in ref 36, but assuming "room temperature" the viscosity of ethanol is 1.20 cp at 20 °C compared with 1.02 cp for cyclohexane at 17 °C.[55] The solvent dependence seen here is reminiscent of the rate increases observed for the isomerization of cis and trans stilbene in alcohol solvents when compared with alkane solvents of comparable viscosity.[3,56−59]

Energy Partitioning in cZt-HT and cZc-HT. Interpretation of the above fitting parameters is complicated by a consideration of the energy partitioning in highly excited cZc-HT and cZt-HT. The harmonic oscillator approximation allows calculation of the average energy content for each vibrational mode of a hot molecule. At a temperature, *T*, the average energy stored in a harmonic vibration of frequency $\bar{\nu}$ in excess of the zero-point energy is given by

$$\langle E(\bar{\nu},T)\rangle = \sum_{n=0}^{\infty} e^{-n\bar{\nu}/k_B T}(1 - e^{-\bar{\nu}/k_B T})n\bar{\nu} \qquad (14)$$

Note that the C−C torsional frequency of *cis*-hexatriene is approximately 100−150 cm^{-1}. The frequencies obtained from the analysis of the time dependent quantum yields range from 40 to 130 cm^{-1}. For such low-frequency vibrations, the average excess energy per mode will not drop below 700 cm^{-1} until the internal temperature reaches 1000−1100 K or 400 cm^{-1} until the internal temperature reaches 600 to 700 K. These calculations lead to the conclusion that Z-HT is prepared on the ground state surface with an average energy content per torsional mode that is less than the calculated 1809 cm^{-1} barrier for isomerization from tZt → cZt. On the other hand, at early times cZt will be produced with an average energy content per torsional mode that is substantially greater than the calculated 721 cm^{-1} barrier for isomerization from cZt → tZt. Likewise cZc-HT will be produced with an average energy content per torsional mode that is far in excess of the calculated 414 cm^{-1} barrier for isomerization from cZc → cZt. It should be noted that Kramer's theory is derived for barrier heights in excess of kT.

Because the barriers for t → c isomerization are in excess of kT, a three-state model invoking transition states between cZc-HT, cZt-HT, and tZt-HT may remain appropriate in the limit of ultrafast energy redistribution. That is, it is possible to define a point upon the reaction pathway between s-cis and s-trans configurations having an infinitesimal lifetime, where spectroscopically identifiable products are located to the right and spectroscopically identifiable reactants are located to the left. Such an interpretation is consistent with the experimental observations presented above. However, the high internal temperature complicates the interpretation of the fitting parameters in terms of a barrier crossing process, and a more sophisticated dynamical modeling may be required.

Conclusion

This paper has reported a femtosecond transient absorption investigation of the ground and excited-state dynamics of *cis*-1,3,5-hexatriene (Z-HT) and 1,3-cyclohexadiene following excitation to the strongly allowed 1^1B state in cyclohexane and n-hexadecane solvents. The internal conversion from the excited state manifold to produce vibrationally excited Z-HT is essentially solvent independent and occurs with rates of ca. 2 to 4 ps^{-1}. The ability to produce vibrationally hot Z-HT with different initial energy distributions and different initial geometries has been expoited to explore the competition between conformational relaxation, intramolecular energy redistribution and thermalization in condensed phases.

The transient absorption results presented above demonstrate that the energy relaxation and conformational relaxation dynamics of Z-HT are similar in cyclohexane and hexadecane. The decay of the initial photoproduct and appearance of the total cZt-HT plus tZt-HT products following excitation of CHD are in excellent agreement with the rise of the 1625 cm^{-1} ethylenic stretching vibration in the time-resolved resonance Raman measurements of Mathies and co-workers.[20−23] It is clear from these data, that the "dark" intermediate state in the resonance Raman experiment and the initial photoproduct state observed in transient absorption experiment are the same. The assignment of this state to Z-HT in the electronically excited 2^1A state or cZc-HT in the ground electronic state is not unambiguous. Vapor phase ionization measurements support the assignment to cZc-HT.[25−26]

Interesting solvent differences are observed when the data reported in this paper are compared with that reported by Lochbrunner et al. for CHD and Z-HT in ethanol.[19] Following excitation of Z-HT, the magnitude of the population trapped as cZt-HT is substantially smaller in ethanol than in cyclohexane or hexadecane. This difference is most apparent when the residual transient absorption difference spectra between 40 and 80 ps reported in Figure 7 of ref 19 are compared with the transient difference spectra reported in Figure 2 above. The smaller residual population implies a substantially faster rate constant for the cZt-HT → tZt-HT reaction.

A similar solvent effect is observed for the cZc-HT → cZt-HT reaction following excitation of CHD in ethanol, cyclohexane and hexadecane. The data and analysis suggest a ca. 4-fold decrease in the lifetime of the initial photoproduct in ethanol as compared with cyclohexane and hexadecane. The solvent dependence deduced from these data sets are reminiscent of the solvent dependences observed for cis- and *trans*-stilbene in alcohol and alkane solvents.

Acknowledgment. This work is supported by a grant from the NSF (Grant CHE-9415772). S.H.P. was supported by the NSF through the Center for Ultrafast Optical Science, under grant STC PHY 8920108.

Supporting Information Available: Plots of kinetic measurements obtained following excitation of 1,3-cyclohexadiene and 1,3,5-*cis*-hexatriene in hexadecane solvent (2 figures), a plot of the evolution of the difference spectrum following excitation of 1,3-cyclohexadiene in cyclohexane solvent also included, the evolution of the difference spectrum differs slightly from that presented earlier (ref 27) (4 pages). Ordering information is given on any current masthead page.

References and Notes

(1) For reviews, see: Waldeck, D. H. *Chem. Rev.* **1991**, *91*, 415. Saltiel, J.; Charlton, J. L. In *Rearrangements in Ground and Excited States*; Vol. 3; de Mayo, P., Ed.; Academic Press: New York, 1980; Vol. 3 p 25. Saltiel, J.; Sun, Y.-P. In *Photochromism Molecules and Systems*; Dürr, H., Bouas-Laurent, H., Eds.; Elsevier: Amsterdam, 1990; p 64. Schroeder, J.; Troe, J. In *Activated Barrier Crossing. Applications in Physics, Chemistry and Biology*; Fleming, G. R., Hänggi, P., Eds.; World Scientific: Singapore, 1993; p 206.

(2) Raftery, D.; Sension, R. J.; Hochstrasser, R. M. In *Activated Barrier Crossing. Applications in Physics, Chemistry and Biology*; Fleming, G. R., Hänggi, P., Eds.; World Scientific: Singapore, 1993; p 163.

(3) Todd, D. C.; Fleming. G. R. *J. Chem. Phys.* **1993**, *98*, 269.

(4) Bondybey, V. E. *Annu. Rev. Phys. Chem.* **1984**, *35*, 591.

(5) Seilmeier, A.; Kaiser, W. In *Ultrashort Laser Pulses and Applications*; Kaiser, W., Ed.; Springer: Berlin, 1988; p 279.

(6) Elsaesser, T.; Kaiser, W. *Annu. Rev. Phys. Chem.* **1991**, *42*, 83.

(7) Owrutsky, J. C.; Raftery, D.; Hochstrasser, R. M. *Annu. Rev. Phys. Chem.* **1994**, *45*, 519.

(8) Sension, R. J.; Szarka, A. Z.; Hochstrasser, R. M. *J. Chem. Phys.* **1992**, *97*, 5239. Sension, R. J.; Repinec, S. T.; Szarka, A. Z.; Hochstrasser, R. M. *J. Chem. Phys.* **1993**, *98*, 6291.

(9) Matousek, P.; Parker, A. W.; Toner, W. T.; Towrie, M.; de Faria, D. L. A.; Hester, R. E.; Moore, J. N. *Chem. Phys. Lett.* **1995**, *237*, 373.

(10) Qian, J.; Schultz, S. L.; Jean, J. M. *Chem. Phys. Lett.* **1995**, *233*, 9.

(11) Schultz, S. L.; Qian, J.; Jean, J. M. *J. Phys. Chem. A.* **1997**, *101*, 1000.

(12) Hayden, C. C.; Chandler, D. W. *J. Phys. Chem.* **1995**, *99*, 7897.

(13) Cyr, D. R.; Hayden, C. C. *J. Chem. Phys.* **1996**, *104*, 771.

(14) Ohta, K.; Naitoh, Y.; Saitow, K.; Tominaga, K.; Hirota, N.; Yoshihara, K. *Chem. Phys. Lett.* **1996**, *256*, 629.

(15) Pullen, S. H.; Anderson, N. A.; Walker, L. A., II; Sension, R. J. *J. Chem. Phys.* **1997**, *107*, 4985.

(16) Fuss, W.; Schikarski, T.; Schmid, W. E.; Trushin, S. A.; Hering, P.; Kompa, K. L. *J. Chem. Phys.* **1997**, *106*, 2205.

(17) Lochbrunner, S.; Fuss, W.; Schmid, W. E.; Kompa, K.-L. *Chem. Phys. Lett.* **1997**, *274*, 491.

(18) Ohta, K.; Naitoh, Y.; Tominaga, K.; Hirota, N.; Yoshihara, K. *J. Phys. Chem. A* **1998**, 102, 35.

(19) Lochbrunner, S.; Fuss, W.; Schmid, W. E.; Kompa, K.-L. *J. Phys. Chem. A* **1998**, *102*, 9334.

(20) Reid, P. J.; Doig, S.; Mathies, R. A. *Chem. Phys. Lett.* **1989**, *156*, 163.

(21) Reid, P. J.; Doig, S.; Mathies, R. A. *J. Phys. Chem.* **1990**, *94*, 8396.

(22) Reid, P. J.; Doig, S. J.; Wickham, S. D.; Mathies, R. A. *J. Am. Chem. Soc.* **1993**, *115*, 4754.

(23) Reid, P. J.; Lawless, M. K.; Wickham, S. D.; Mathies, R. A. *J. Phys. Chem.* **1994**, *98*, 5597.

(24) Pullen, S. H.; Walker, L. A., II.; Donovan, B.; Sension, R. J. *Chem. Phys. Lett.* **1995**, *242*, 415.

(25) Fuss, W.; Schikarski, T.; Schmid, W. E.; Trushin, S. A.; Kompa, K. L. *Chem. Phys. Lett.* **1996**, 262, 675.

(26) Trushin, S. A.; Fuss, W.; Schikarski, T.; Schmid, W. E.; Kompa, K. L. *J. Chem. Phys.* **1997**, *106*, 9386.

(27) Pullen, S. H.; Anderson, N. A.; Walker, L. A., II.; Sension, R. J. *J. Chem. Phys.* **1998**, *108*, 556.

(28) Fuss, W.; Höfer, T.; Hering, P.; Kompa, K. L.; Schikarski, T.; Schmid, W. E. *J. Phys. Chem.* **1996**, *100*, 921.

(29) Bernardi, F.; De, S.; Olivucci, M.; Robb, M. A. *J. Am. Chem. Soc.* **1990**, *112*, 1737.

(30) Olivucci, M.; Bernardi, F.; Celani, P.; Ragazos, I.; Robb, M. A. *J. Am. Chem. Soc.* **1994**, *116*, 1077.

(31) Celani, P.; Ottani, S.; Olivucci, M.; Bernardi, F.; Robb, M. A. *J. Am. Chem. Soc.* **1994**, *116*, 10141.

(32) Celani, P.; Bernardi, F.; Robb, M. A.; Olivucci, M. *J. Phys. Chem.* **1996**, *100*, 19364.

(33) Garavelli, M.; Celani, P.; Bernardi, F.; Robb, M. A.; Olivucci, M. *J. Am. Chem. Soc.* **1997**, *119*, 6891.

(34) Garavelli, M.; Celani, P.; Bernardi, F.; Robb, M. A.; Olivucci, M. *J. Am. Chem. Soc.* **1997**, *119*, 11487.

(35) Celani, P.; Bernardi, F.; Olivucci, M.; Robb, M. A. *J. Am. Chem. Soc.* **1997**, *119*, 10815.

(36) Vreven, T.; Bernardi, F.; Garavelli, M.; Olivucci, M.; Robb, M. A.; Schlegel, H. B. *J. Am. Chem. Soc.* **1997**, *119*, 12687.

(37) Kramers, H. A. *Physica* **1940**, *7*, 284.

(38) Chandrasekhar, S. *Rev. Mod. Phys.* **1943**, *15*, 1.

(39) Hänggi, P.; Talkner, P.; Borkovec, M. *Rev. Mod. Phys.* **1990**, *62*, 251.

(40) Pullen, S.; Walker, L. A. II; Sension, R. J. *J. Chem. Phys.* **1995**, *103*, 7877.

(41) Hwa, J. C. H.; de Benneville, P. L.; Sims, H. J. *J. Am. Chem. Soc.* **1960**, *82*, 2537.

(42) Minnaard, N. G.; Havinga, E. *Recl. Trav. Chim.* **1973**, *92*, 1315.

(43) Buma, W. J.; Kohler, B. E.; Song, K. *J. Chem. Phys.* **1991**, *94*, 6367.

(44) Orchard, S. W.; Thrush, B. A. *Proc. R. Soc. London A.* **1974**, *337*, 257.

(45) Frisch, M. J.; Trucks, G. W.; Schlegel, H. B.; Gill, P. M. W.; Johnson, B. G.; Robb, M. A.; Cheeseman, J. R.; Keith, T.; Petersson, G. A.; Montgomery, J. A.; Raghavachari, K.; Al-Laham, M. A.; Zakrzewski, V. G.; Ortiz, J. V.; Foresman, J. B.; Peng, C. Y.; Ayala, P. Y.; Chen, W.; Wong, M. W.; Andres, J. L.; Replogle, E. S.; Gomperts, R.; Martin, R. L.; Fox, D. J.; Binkley, J. S.; Defrees, D. J.; Baker, J.; Stewart, J. P.; Head-Gordon, M.; Gonzalez, C.; Pople, J. A. *Gaussian 94*, Revision B.3; Gaussian, Inc.: Pittsburgh, PA, 1995.

(46) Panchenko, Y. N.; Kranoshchiokov, V.; George, P.; Bock, C. W. *Struct. Chem.* **1992**, *3*, 15.

(47) Liu, R.; Zhou, X. *J. Phys. Chem.* **1993**, *97*, 1850.

(48) Furukawa, Y.; Takeuchi, H.; Harada, I.; Tasumi, M. *J. Mol. Struct.* **1983**, *100*, 341.

(49) Yoshida, H.; Furukawa, Y.; Tasumi, M. *J. Mol. Struct.* **1989**, *194*, 279.

(50) Minnaard, N. G.; Havinga, E. *Recl. Trav. Chim.* **1973**, *92*, 1179.

(51) (a) Gavin, R. M.; Risemberg, S.; Rice, S. A. *J. Chem. Phys.* **1973**, *58*, 3161. (b) Gavin, R. M. Jr.; Rice, S. A. *J. Chem. Phys.* **1974**, *60*, 3231.

(52) Carreira, L. A. *J. Chem. Phys.* **1975**, *62*, 3851.

(53) Ackerman, J. R.; Kohler, B. E. *J. Chem. Phys.* **1984**, *80*, 45.

(54) Karpfen, A.; Choi, C. H.; Kertesz, M. *J. Phys. Chem. A* **1997**, *101*, 7426.

(55) Lide, D., Ed.; *Handbook of Chemistry and Physics*; CRC Press: Boca Raton, FL, 1991; Vol. 22.

(56) Sundstrom, V.; Gillbro, T. *Chem. Phys. Lett.* **1984**, *109*, 538.

(57) Courtney, S. H.; Fleming, G. R. *J. Chem. Phys.* **1985**, *83*, 215.

(58) Courtney, S. H.; Kim, S. K.; Canonica, S.; Fleming, G. R. *J. Chem. Soc., Faraday Trans.* **1986**, *82*, 2065.

(59) Hicks, J. M.; Vandersall, M. T.; Sitzmann, E. V.; Eisenthal, K. B. *Chem. Phys. Lett.* **1987**, *135*, 413.